Accepted Manuscript

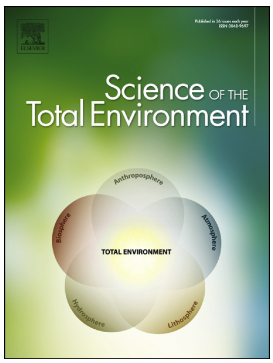

Bioretention cells under cold climate conditions: Effects of freezing and thawing on water infiltration, soil structure, and nutrient removal

Brenden Ding, Fereidoun Rezanezhad, Behrad Gharedaghloo, Philippe Van Cappellen, Elodie Passeport

PII: S0048-9697(18)33337-0
DOI: doi:10.1016/j.scitotenv.2018.08.366
Reference: STOTEN 28428

To appear in: *Science of the Total Environment*

Received date: 21 May 2018
Revised date: 22 August 2018
Accepted date: 26 August 2018

Please cite this article as: Brenden Ding, Fereidoun Rezanezhad, Behrad Gharedaghloo, Philippe Van Cappellen, Elodie Passeport , Bioretention cells under cold climate conditions: Effects of freezing and thawing on water infiltration, soil structure, and nutrient removal. Stoten (2018), doi:10.1016/j.scitotenv.2018.08.366

Bioretention cells under cold climate conditions: Effects of freezing and thawing on water infiltration, soil structure, and nutrient removal

Brenden Ding[a], Fereidoun Rezanezhad[b], Behrad Gharedaghloo[c], Philippe Van Cappellen[b], Elodie Passeport*[a,d]

[a] *Department of Civil and Mineral Engineering, University of Toronto, 35 St George St, Toronto, ON, M5S 1A4, Canada*

[b] *Ecohydrology Research Group, Water Institute and Department of Earth & Environmental Sciences, University of Waterloo, 200 University Avenue West, Waterloo, ON N2L 3G1, Canada*

[c] *Department of Geography and Environmental Managements, University of Waterloo, 200 University Avenue West, Waterloo, ON N2L 3G1, Canada*

[d] *Department of Chemical Engineering and Applied Chemistry, University of Toronto, 200 College St, Toronto, ON M5S 3E5, Canada*

* Corresponding author:

email: elodie.passeport@utoronto.ca; phone: +1 416 978 5747

Abstract

Bioretention cells are a popular control strategy for stormwater volume and quality, but their efficiency for water infiltration and nutrient removal under cold climate conditions has been poorly studied. In this work, soil cores were collected from an active bioretention cell containing engineered soil material amended with a phosphate sorbent medium. The cores were used in laboratory column experiments conducted to obtain a detailed characterization of the soil's bioretention performance during six consecutive freeze – thaw cycles (FTCs, from −10 to + 10 °C). At the start of each FTC, the experimental column undergoing the FTCs and a control column kept at room temperature were supplied with a solution containing 25 mg/L of bromide, nitrate and phosphate. Water saturated conditions were established to mimic the presence of an internal water storage zone to support anaerobic nitrate removal. At the end of each FTC, the pore solution was allowed to drain from the columns. The results indicate that the FTCs enhanced the infiltration efficiency of the soil: with each successive cycle the drainage rate increased in the experimental column. Freezing and thawing also increased the saturated hydraulic conductivity of the bioretention soil. X-ray tomography imaging identified a key role of macro-pore formation in maintaining high infiltration rates. Both aqueous nitrate and phosphate supplied to the columns were nearly completely removed from solution. Sufficiently long retention times and the presence of the internal water storage zone promoted anaerobic nitrate elimination despite the low temperatures. Dissolved phosphate was efficiently trapped at all depths in the soil columns, with ≤ 2% of the added stormwater phosphate recovered in the drainage

effluent. These findings imply that, when designed properly, bioretention cells can support high infiltration rates and mitigate nutrient pollution in cold climates.

Keywords

Bioretention cells; infiltration; nitrate; phosphate; freeze – thaw cycles; pollution

1. Introduction

Bioretention cells are urban stormwater control systems made of a depression in the ground, typically covered by mulch and a wide range of plants, and where the original soil has been replaced by an engineered medium designed to enhance water infiltration and promote contaminant removal. Bioretention cell efficiency for nutrient removal and water infiltration has been extensively studied under temperate climate conditions (Hunt et al., 2012; Roy-Poirier et al., 2010). Even though nitrogen and phosphorus removal rates are often strongly variable, specific design strategies have proven effective at limiting nutrient export out of the system. For example, the implementation of a saturated internal water storage zone can be used to support denitrification (Dietz and Clausen, 2006; Kim et al., 2003), and various engineered media amendments, such as fly-ash, water treatment residual, red mud, and alum can be added to promote sustainable phosphorus adsorption (Lucas and Greenway, 2011; O'Neill and Davis, 2012; Yan et al., 2016; Zhang et al., 2008). Conversely, the performance of bioretention cells is not well known. Freezing and thawing cycles (FTCs) in particular are known to affect natural soil structure by destabilizing soil aggregates, in particular for soils with high water contents. The relocation of destabilized aggregates can clog some of the soil pores and reduce the infiltration capacity (Hayashi, 2013). Moreover, FTCs typically affect microbial activity and diversity and therefore the speciation and mobility of various chemical elements (Campbell et al., 2005; Matzner and Borken, 2008). Even though lower temperatures result in slower microbial activity, the breaking of soil aggregates and mortality of microorganisms and plant roots during FTCs

produce readily bioavailable organic carbon that support denitrification upon thawing (Christensen and Christensen, 1991).

Engineered soil media used in bioretention cells have a high sand content in order to maintain high hydraulic conductivity. For example, in southern Ontario, bioretention media are recommended to consist of 85 – 88 % sand (0.050 – 2.0 mm), 8 – 12 % fines (< 0.050 mm), and 3 – 5 % organic matter, and to support infiltration rates greater than 25 mm/h (Dhalla and Zimmer, 2010). In such sandy soil media, the effects of freezing and thawing on soil structure and nutrient removal are unclear due to a lack of research on the topic. For countries where winter temperatures are frequently below freezing, a better characterization of FTC effects on bioretention performance is critical to guarantee their functioning throughout the year, especially during early winter and early spring when repeated soil freezing and thawing is a common occurrence.

To date, some studies have described the performance of bioretention cells under cold temperate climate conditions, but for soil temperature > 0°C (e.g., Blecken et al. (2010), Khan et al. (2012a; 2012b)). However, many research gaps still exist (Kratky et al., 2017). In particular, very limited research has incorporated experimental conditions leading to successive freezing (soil surface temperature < 0°C) and thawing (soil surface temperature > 0°C) of bioretention soils (Al-Houri et al., 2009; Denich et al., 2013; Géhéniau et al., 2015; Moghadas et al., 2016; Muthanna et al., 2007; Muthanna et al., 2008; Valtanen et al., 2017). Several authors reported reduced infiltration rates during the freezing period due to a reduction in pore availability (Al-Houri et al., 2009; Muthanna et al., 2008), and increased infiltration rates upon thawing (Denich et al., 2013; Moghadas et al., 2016; Valtanen et al., 2017). However, the latter results are mostly of a descriptive nature, with no definitive

explanation of the observations. Mechanism-oriented research is needed to characterize hydrological and contaminant transfer and transformation processes in bioretention cells undergoing freezing and thawing cycles (Kratky et al., 2017).

The methodologies used in soil FTC experiments have taken many forms, which makes it difficult to compare results among various experiments and relate them to real field conditions (Henry, 2007). Frost depths are usually limited to the top few centimetres of the soil due to the temperature buffering effect of snow cover, soil, mulch, and vegetation (Henry, 2007). Indeed, sub-zero air temperatures do not necessarily translate into sub-zero temperatures across the soil profile (Fach et al., 2011). A review by Henry (2007) reported that soils rarely freeze below 5 cm in depth, even though deeper frost depths, up to 20 cm have been observed both in natural (Henry (2007) and references therein) and bioretention soils (Géhéniau et al., 2015; Roseen et al., 2009; Valtanen et al., 2017). Occasionally, in some areas of the world such as in west Canada, frost depths are highly variable and can go down to −45 cm (Christensen et al., 2013; He et al., 2015). The number, frequency, and amplitude of FTCs, as well as the target freezing temperature and the rate at which this temperature is first reached can have irreversible negative impacts on soil microorganisms and result in larger than expected effects on parameters and processes, such as soil structure and nutrient fate and transport (Henry, 2007).

In the present study, an experimental soil column set-up was used to freeze / thaw the top 5 cm in an undisturbed soil core collected from an active bioretention cell in a cold climate region. By imposing successive cycles of freezing and thawing on the bioretention soil column, the objectives of this study were to (1) characterize changes in bioretention infiltration capacity and soil structure, and (2) quantify the retention efficiencies of aqueous

nitrate (NO_3^-) and phosphate (PO_4^{3-}) supplied at the top of the columns. In order to relate the observations to the FTCs, a control experiment with a column containing the same soil, but maintained at a constant room temperature, was also carried out.

2. Materials and Methods

2.1 Bioretention cell site and sample collection

Soil samples were collected in September 2015 from a bioretention cell located in Ajax, Ontario, Canada and installed between October and November 2014 (Appendix A: Supplemental Material (SM) Figure S1). The site is located in an urban catchment with a contributing 95% impervious area and receives runoff from a 4,160-m^2 drainage area. The bioretention cell surface area is 488 m^2 and the depth of the engineered soil medium is 50 cm. The soil had mulch at the top and, prior to installation, was amended with a medium enriched in iron and aluminum oxides (Sorbtive® media, Imbrium Systems), in a proportion of 3.1% by volume, for enhanced phosphorus removal. Four undisturbed soil cores of 7.5 cm inner diameter and 45 cm length were sampled by manually pushing into the soil a custom-made coring tube, fitted with a top cap to hold the soil in place upon retrieval. The soil cores were taken approximately 5 cm apart from each other to ensure the columns had comparable grain size distributions and received similar stormwater runoff loadings. No rooted vegetation was present where the samples were collected and more than 50% of the bioretention surface had no plants and only mulch on top of the soil. The soil samples were immediately transported to the laboratory for the experiments.

2.2 Experimental setup

Three of the soil cores were used. They were inserted into the columns from the bottom by a custom-made lifting jack device that resulted in minimal disturbance (SM Figure S1). One core, the control column (CC), remained at room temperature, 22.9 ± 0.6 °C, throughout the entire experiment. Another core, the experimental FTC column (EC) was placed in an environmental chamber whose air temperature was controlled. The third core, referred to as the initial column, was sliced at 3 cm depth intervals to determine solid phase total organic carbon (TOC), total nitrogen (TN) and total phosphorus (TP). Given that the engineered soil was homogenized before installation in the bioretention cell, and that the cores were collected near each other, the compositional data obtained on the third (initial) core were considered adequate surrogates for the initial soil properties of the other two soil cores.

In order to evaluate the effects of multiple FTC on bioretention performance, long-term experiments, consisting of six successive replicate injection experiments, were conducted. Contrary to single-injection short-term experiments in which replicates are key to draw reliable conclusions, the approach used in this study was validated by the consistency observed among the six time-series data. Moreover, in addition to the EC subject to FTC, the CC acted as a reference point to compare the EC results to. The CC also received six injections of the same injection solution and following the same schedule as for the EC. The CC and EC consisted of 45 cm bioretention soil to which 5 cm of mulch and plant debris from the site were added on top (Figure 1 and SM Figure S1). The CC and EC exhibited very similar particle size distributions, with 96-98% of particle mass in the sand fraction (SM Figure S4 and Table S3). No living plants were present in the soil cores to

best represent field winter conditions. A 150-W band heater was wrapped around the lower portion of the EC to maintain the temperature at 8 °C, which is representative of southern Ontario's subsurface soil and groundwater temperatures (Conant, 2004; Gunther, 1980), leaving the top 5 cm of soil exposed to the chamber air temperature, which cycled between −10 and +10 °C (see below for details). In addition, approximately 5 cm of artificial snow was added on top of the EC at the beginning of each freezing period. The snow was equivalent to 94.4 ± 0.4 mL of water in each injection experiment, contributing to diluting the EC solute concentrations by approximately 23% compared to the CC (SM Figure S2). The use of the band heater, the absence of living plants, and the addition of the snow were chosen to simulate realistic winter conditions where the freezing depth is limited to the top of the soil, no living plants are present, and the snow acts as an insulation layer and provides dilution of contaminant concentrations upon thawing in the field.

Porewater Micro-Rhizon samplers 5 cm in length and 2.5 mm in diameter (CSS5 MicroRhizon™ samplers, Ejikelamp, Netherlands) were introduced horizontally into the soil matrix, at depths of 1, 4.5, 11, 23, and 32 cm below the soil surface in both columns. For each FTC, soil porewater samples were extracted 24 hours after the start of the 3-day long freezing period, 5 hours after the start of the 4-day long thawing period, and 24 hours after the end of the thawing period. After 1.5 days of thawing, the drainage on/off valves located at the bottom of each column were fully opened to allow for gravitational draining. Drainage effluent samples were collected every 5 to 60 min by letting the drainage water directly flow into graduated sample collection tubes, and drainage rates were measured by recording the outflow volumes from the columns over time. Only the drainage rates of the

first five cycles (FTC 1 – FTC 5) were measured, as the drainage outlet of the EC malfunctioned during the last thawing period.

2.3 Injection solution

An injection solution containing 25 mg/L each of PO_4^{3-} (8.33 mg/L of PO_4^{3-}-P), NO_3^- (5.65 mg/L of NO_3^--N), and bromide (Br^-) was prepared in 0.01 M calcium chloride ($CaCl_2$) to mimic highly contaminated surface runoff entering the bioretention cell, and a typical soil solution ionic strength (OECD, 2004) (SM Table S1). Note that the PO_4^{3-} and NO_3^- concentrations were higher than typically found in average stormwater (Lee and Bang, 2000; Passeport et al., 2009). This was selected to test the bioretention performance under extreme nutrient loading conditions, thus placing the study in a worst-case scenario for water quality.

2.4 Freeze – thaw cycles

A total of six consecutive FTCs were conducted. Prior to the start of each FTC, the injection solution was added from the top into the EC and CC to the point of saturation, in order to mimic a bioretention cell design with an internal water storage zone. The soil was considered saturated when the water level just covered the plant debris in each column. In the field, internal water storage zones are typically designed below the top 10 to 30 cm of the soil. In this study, the whole depth of each soil column was saturated to evaluate the maximum effects of FTC, which were only applied to the top of the EC column. Note that the injection solution was added from the top of the columns, thus possibly leaving some air entrapped into the soils. The injection solution was allowed to drain out of the columns

at the end of each FTC, that is, upon thawing of the upper soil in the EC. Following the recommendations of Henry (2007), the temperature of the environmental chamber containing the EC was progressively lowered from room temperature to 0 °C over a span of 14 days to prevent the soil from undergoing an abrupt temperature shock. Once stabilized at 0 °C, the EC underwent a series of six FTCs, consisting of chamber air temperature cycles of −10 °C for 3 days (freezing) followed by +10 °C for 4 days (thawing). The corresponding temporal soil temperature profiles are shown in SM Figure S3.

2.5 Aqueous sample analytical methods

Aqueous samples collected from the five depths and the drainage effluents of the soil columns were filtered through 0.2-μm pore size membrane filters (Thermo Scientific Polysulfone filter) for analysis of NO_3^-, PO_4^{3-}, Br^-, and sulphate (SO_4^{2-}, note that the injection solution did not contain SO_4^{2-}) by Ion Chromatography (IC, Dionex ICS-5000). One mL of each filtered sample was diluted and acidified with 2% HNO_3 for analysis of total dissolved phosphorus (TDP), total dissolved iron (TDFe), total dissolved manganese (TDMn), and total dissolved sulphur (TDS) concentrations using Inductively-Coupled Plasma Optical Emission Spectroscopy (Thermo iCAP 6200 Duo ICP/OES). Concentrations of total dissolved nitrogen (TDN), dissolved organic carbon (DOC), and dissolved inorganic carbon (DIC) were measured using the non-purgeable organic carbon method on a total organic carbon analyzer (Shimadzu TOC-LCPH/CPN). Samples for DOC analysis were mixed with 20 μL of 1 M HCl. Further details on the method detection limits (MDL) and limits of quantification (LOQ) are provided in SM Section S5 and Table S2.

2.6 Soil chemical and physical characterization

Before the first artificial stormwater injection experiment, a 200-mL volume of 0.01 M $CaCl_2$ with no other chemicals was injected and allowed to drain gravitationally to compare the initial drainage rates of both columns (SM Section S6 Figure S5). At the end of the experiments, the soil columns were fully drained, extruded, and sliced every 3 cm. An undisturbed soil core sample was collected near the top (depth interval: −2 to −4 cm) of both the CC and EC. Note that only the top 5 cm of the EC soil experienced freezing and thawing. The samples were analyzed by X-ray tomography with a Skyscan 1173 X-ray micro-computed tomography (XR-μCT) instrument, using an 80 kV X-ray source, a current of 100 mA, and a resolution of 13.15 × 13.15 × 13.15 μm for each voxel. Further details on the analytical method and porosity parameter determination are provided in SM Section S5. The remaining soil slices were homogenized and separate aliquots were freeze-dried and stored at room temperature before analysis for soil TOC, TP, and TN concentrations at the University of Guelph, Laboratory Services, Agriculture and Food Laboratory, ON, Canada (SM Section S5).

2.7 Saturated hydraulic conductivity

Another four undisturbed soil cores of 80 mm diameter × 50 mm height each were collected from the same site in October 2016. The soil cores were capped at the top and bottom and were transported to the lab to study the effect of FTCs on the soil's saturated hydraulic conductivity (K_{sat}). The caps were removed from both ends, and a ring with a porous plate was fitted at the bottom of each core. The soil cores were first saturated from the bottom by placing them in a tray where tap water was added. They were then placed in

a freezer at −5 °C to freeze for 2 days to simulate comparable temperature conditions as for the EC, before being allowed to thaw at room temperature. This was repeated until the K_{sat} values were above the measurable K_{sat} value of the instrument for all soil samples, i.e., 11,050 cm/d. Triplicate measurements of the K_{sat} values were done for each of the four replicate cores using a UMS K_{sat} Benchtop Saturated Hydraulic Conductivity Instrument.

3. Results

3.1 Drainage hydraulics

As shown in SM Figure S5, the initial drainage properties of both columns were similar before the start of the injection experiments. The peak flow rate of the EC was slightly higher (2.5 mL/min or 34 mm/h) and sooner (29.5 min) than that of the CC (2.3 mL/min or 31 mm/h and 35.5 min, respectively), and the EC flow rate stopped sooner (143 min) than that of the CC (280 min). At the end of each injection experiment, the average drainage rates of the EC were always higher than for the CC, at 1.99 ± 0.06 *versus* 0.81 ± 0.16 mL/min, corresponding to 27 ± 1 *versus* 11 ± 2 mm/h (Figure 2). The drainage rates reached 0.5 mL/min in the EC and the CC after 4 h and 3 h, respectively, and 50% of the water volume drained out of the columns in less than ~2 h. Therefore, the hydraulic retention time was approximately 4 days. In two consecutive injection experiments, the average drainage rates decreased by 11 ± 8 % (n = 4) in the CC but increased by 1.7 ± 3.0 % (n = 4) in the EC. Overall, comparing the average drainage rates between FTC 1 and FTC 5, the CC showed a 37% decrease, whereas the EC saw a 6.8% increase. The decrease in the CC drainage rate was likely the result of clogging. Note that no particulate matter

was added in the injection solution. Therefore, clogging in the CC was likely due to the relocation of fine particles to lower depths. This, however, was not detected in the EC, suggesting that the alternation of freezing and thawing in the top zone of the EC was able to counteract potential clogging.

The trends in drainage rate results observed in the EC are in line with the K_{sat} values measured on the four additional soil cores collected at the same site. While the four soil samples had different initial K_{sat} values, ranging from 1,320 ± 70 to 8,160 ± 2,700 cm/d, they all exhibited a sharp increase and reached the instrument measurable limit of 11,050 cm/d after only three FTCs (SM Figure S6). In other words, the FTCs resulted in an increase of the saturated hydraulic conductivity of the bioretention soil after thawing.

3.2 X-ray tomography results

The results of X-ray tomography analysis for the top undisturbed soil core samples of the control and experimental columns are presented in Table 1, Figure 3 and Appendix B.

The specific surface area in the upper 2-4 cm depth interval of the EC soil was lower than in the corresponding depth interval of the CC soil. In addition, the average pore hydraulic radius, the number of pores, and the average spatial pore density of the EC were higher than those of the CC. Since both columns were made of the same soil collected and transported to the lab under the same conditions, these differences between the EC and the CC can be attributed to the FTCs applied to the EC. During freezing, frost expansion increases porewater pressure leading to higher internal stress and soil grain relocation, thus deforming the soil pore structure (Ma et al., 2015). Since the bulk volume and the total volume of soil grains were constant during FTCs, grain relocation caused the merging and shrinking of pores surrounding the relocated grains. Grain relocation and pore deformation can cause an increase of the average pore radius size and the spatial pore density as observed in the EC (Zhai et al., 2017).

As can be seen in Figure 3, in the CC the pores were uniformly distributed in space and the pore sizes were larger and connected. Conversely, the EC exhibited two groups of pores: one group of larger pores, which likely formed through the combination of large pores, and another group of small pores and isolated pores that presumably formed due to relocation of the soil grains during the FTCs. The pore size statistics confirmed this interpretation: the average pore size in the EC was higher than in the CC, whereas the median pore size was smaller in the EC (Table 1). This indicates that the frequency of small pores was larger in the EC. Given that the maximum pore size was higher in the EC, it follows that the range of pore sizes was broader in the EC compared to the CC. These results demonstrate that the factor porosity alone, i.e., the portion of non-solid material in the soil, is not a representative indicator of the soil pore geometry and resulting infiltration capacity, as it

was lower for the EC, at 32.5 %, than for the CC at 39.8 %. All these results therefore show that FTCs resulted in an increase in the size of the originally large pores and an increase in the frequency of small pores, which together explained the wider pore radius range in the EC.

3.3 Drainage effluent and porewater chemistry

Drainage effluent concentration data are presented in Figure 4 and porewater profiles are shown in Figure 5 and SM Figures S8 and S9. Even during the freezing periods, porewater samples could still be collected up to −1 cm in the EC, indicating only partial freezing of the top soil in the EC. The solution injected at the start of a FTC remained in the columns for 4 days before the onset of drainage. The pH values of both the CC (7.4 ± 0.4) and EC (7.4 ± 0.2) were similar and showed a small decrease of about 0.3 between FTC 1 and FTC 6 (SM Figure S8). In the drainage effluent of both columns, Br^- concentrations averaged 16.9 ± 3.1 mg/L in the first FTC, because of admixing of original porewater to the injection solution supplied to the columns. Thereafter, the concentrations of Br^- measured in the outflow of FTC 2 to 6 approached the stormwater value of 25 mg/L in both columns. The Br^- concentrations at the top of the EC were lower than those injected due to dilution by the snow meltwater produced during thawing. This temporal trend reflects the complete replacement of the initial soil porewater by the added injection solution. The consistency of Br^- concentrations within each column confirms the reliability of the data from this multiple injection experiments.

In both columns, the drainage and porewater NO_3^--N concentrations were more than one order of magnitude lower than the injection solution concentration at 5.65 mg NO_3^--N/L.

The NO_3^--N drainage concentrations exhibited a similar trend as those of Br^- with a slight increase between the first and second FTCs, after which they levelled out at 0.12 ± 0.01 mg/L during the following four FTCs. The much lower NO_3^--N concentrations in the drainage water, relative to the injection solution, indicate active NO_3^- consumption, with more 96% decrease of the injected mass (SM Figure S7). The colder temperatures in the upper 5 cm of soil in the EC compared to the deeper soil maintained at 8 °C, and consequently the lower microbial activity, could explain why the highest NO_3^- porewater concentrations in the EC were found near the soil surface.

While the NO_3^- concentration trends in the EC and CC were quite similar, they differed for TDN. The average drainage TDN value was 2.91 ± 0.78 mg/L for the CC, compared to 0.87 ± 0.55 mg/L observed in the EC drainage. Dilution by the melting snow alone cannot explain the large difference between the two columns. More likely, higher DON concentrations leached out of the CC than the EC. This is consistent with the observed effluent DOC concentrations, which showed very similar differences between the columns as seen for TDN (Figure 4), with significantly higher values for the CC (21.4 ± 5.7 mg/L) than the EC (8.5 ± 2.5 mg/L). In addition, the temporal TDN and DOC trends of the CC tracked one another, with a molar C:N ratio of around 7. Finally, the much lower NO_3^- concentrations (Figure 5) compared to the TDN concentrations (SM Figure S9) suggest that large fractions of TDN were comprised of DON.

From the start of the first drainage period, effluents from both columns had PO_4^{3-}-P concentrations below the MDL of 0.15 mg/L and, therefore, results are not shown in Figure 4. The TDP concentrations were above the MDL of 8.6 µg/L, but below the LOQ at 43 µg/L. While the large differences in TDN between the two columns were not observed for

TDP, the effluent TDP values appeared to be slightly lower for the EC. However, given the very low TDP concentrations, further speculation is not warranted. In both cores, porewater concentrations of TDP were highest in the topmost 5 cm of the soils and decreased with depth. The PO_4^{3-} concentrations showed that other dissolved P species, e.g., dissolved organic P (DOP), contributed significantly to TDP, especially in the CC where porewater PO_4^{3-} concentrations were for the most part below the LOQ. While the porewater TDP concentrations in the CC did not display significant variability among the six injection experiments, in the EC TDP increased progressively over the six FTCs, in particular at the −5 and −11 cm sampling depths (Figure 5). Nonetheless, porewater TDP concentrations remained well below the PO_4^{3-}-P concentration of the injection solution (8.33 mg/L of PO_4^{3-}-P), that is, the injected PO_4^{3-} was efficiently removed from the solution in both the CC and EC. More than 98% of the TDP was removed for both columns and all FTCs (SM Figure S7). The very low TDP (and PO_4^{3-}-P) concentrations in the drainage effluents of the CC and EC (Figure 4) further implied that any remaining porewater TDP was sequestered by the soil during drainage of the columns.

The outflow concentrations of SO_4^{2-}, TDS, TDFe, DIC, DOC, and to a lesser extent TDMn, exhibited systematic differences between the EC and CC (Figure 4). While these differences can be partly attributed to the inherent variability of each soil, the consistency between the replicate injections within each column suggests that the observed differences are due to the FTC imposed to the EC. Relatively high SO_4^{2-}-S concentrations were detected in the drainage effluent from the EC (≥ 3 mg SO_4^{2-}-S/L), with an average value of 3.94 ± 0.73 mg SO_4^{2-}-S/L. Chemical analysis of the artificial snow revealed the presence of SO_4^{2-}, with an average concentration of 8.7 mg SO_4^{2-}-S/L. Assuming no production or

consumption of SO_4^{2-}, this would result in an average concentration of 2.18 mg SO_4^{2-}-S/L in the drainage effluent of the EC. The observed excess SO_4^{2-}-S concentrations in the EC drainage therefore imply production of SO_4^{2-} in the soil. The identical trends of SO_4^{2-}-S and TDS indicate that all aqueous S exported from the EC was under the form of SO_4^{2-}. By contrast, no SO_4^{2-} or TDS leached out of the CC. These trends were confirmed by the porewater TDS and SO_4^{2-}-S concentration profiles. A variety of soil processes can produce porewater SO_4^{2-}. These include the oxidation of reduced minerals and the oxidative or non-oxidative mineralization of organic S (Stevenson, 1986). The porewater profiles of TDS and SO_4^{2-} concentrations further showed decreasing trends from FTC 1 to FTC 6. The decreases were larger in the CC than EC. For example, between FTC 1 and 6 TDS at −32 cm dropped from 9.4 to 4.3 mg/L in the CC, and from 5.1 to 3.2 mg/L in the EC. We speculate that the lack of measurable SO_4^{2-} concentrations in the drainage of the CC was not due to a lack of SO_4^{2-} production. Rather, SO_4^{2-} released to the porewaters of the CC was probably consumed subsequently by microbial SO_4^{2-} reduction. The sulphide produced was further efficiently retained in the CC through formation of iron sulphides or the sulphurization of organic matter (Couture et al., 2013; Rickard and Luther, 2007).

The drainage of the CC also exhibited systematically higher TDFe, DOC and DIC concentrations than the EC. Similar to TDS and SO_4^{2-}, the TDFe and TDMn profiles supported the release of aqueous Fe and Mn to the porewater. The TDFe and TDMn concentrations in the upper part of the EC were much lower than in the CC.

The porewater DIC and DOC concentration profiles showed opposite depth and temporal trends, consistent with mineralization of DOC producing DIC (Figure 5). In general, the DOC concentrations were highest for FTC 1 and 2 and lower for the subsequent FTCs,

while the DIC concentrations were lowest for FTC 1. In addition, the CC exhibited significantly higher porewater DOC concentrations than the EC. Dilution by the melting snow may in part explain the lower TDFe, DOC and DIC concentrations in the EC. However, taken together the differences in solution composition between the EC and CC were consistent with higher microbial activity in the CC that remained at a higher temperature, whereas the experimental column was maintained at 8 °C below the top 5 cm of the soil. Faster enzymatic degradation and mineralization of soil organic matter explain the higher DOC (and TDN) and DIC concentrations in the CC effluents, while reductive dissolution of the ferric iron oxides present in the engineered soil matrix, coupled to organic carbon oxidation, could account for the higher TDFe concentrations for the CC. The porewater data further imply that the inter-column differences in microbial activity were most pronounced in the uppermost soil, where temperature differences were greatest.

3.4 Solid-phase soil chemistry

In Figure 6, the depth distributions of TOC, TP, and TN collected in the EC and CC at the end of the experiment are compared to the corresponding profiles in the initial soil column. As shown by the TOC and TN results, most organic matter in the bioretention soil was concentrated in the upper 10 cm, while TP concentrations peaked around −5 cm. Relative to the initial column, the EC and CC both showed a depletion of TOC and TN. The changes in concentrations were most pronounced in the upper portions of the columns. For instance, the TOC concentration in the 0-3 cm depth interval of the initial column was 410 mg/g, compared to 112 and 174 mg/g for the CC and EC, respectively.

The observed TOC and TN trends support the key role of organic matter degradation in controlling the biogeochemical changes inferred from the drainage and porewater data. The very large decrease in the TOC:TN ratio further implied the preferential degradation of plant-derived organic matter with a high C:N ratio and, possibly, the addition of N-rich microbial biomass (Fenchel et al., 2012). In contrast to TOC and TN, the results implied an accumulation of TP in the EC and CC. The TP concentrations were generally lowest in the initial column, and highest in the CC. The largest increases in TP concentration were observed near the soil surface, with concentrations approaching 1 mg/g. Thus, taken together the aqueous and solid-phase data consistently point to very different removal mechanisms of the NO_3^- and PO_4^{3-} injected into the soil columns.

4. Discussion

4.1 Bioretention hydraulics and soil porosity

This study provides multiple lines of evidence that FTCs may enhance infiltration in bioretention soils. It also illustrates the key role of macro-pore formation by FTCs in maintaining high infiltration rates (> 25 mm/h). An increase in drainage rate following freezing and thawing events, as seen here for the EC, has been reported previously in both indoor and outdoor bioretention soil column studies (Denich et al., 2013; Moghadas et al., 2016; Valtanen et al., 2017). The contrasting decrease in drainage rates in the CC is attributed to clogging by the downward movement of fine particles, a process often observed in bioretention systems (Le Coustumer et al., 2012; Li and Davis, 2008), and which in cold climates could be enhanced by the use of road salts in winter (Kakuturu and

Clark, 2015). As also suggested by Denich et al. (2013), we propose that FTCs counteract clogging, consistent with the observed increases in the saturated hydraulic conductivity of the bioretention soil measured upon thawing after successive freezing events. In bioretention with an unsaturated top zone, series of FTC would likely affect the soil structure and hydrologic regime to a lower extent.

To the best of our knowledge, this study is the first to demonstrate via X-ray tomography imaging that FTCs simultaneously cause the creation of larger pores and increase the frequency of smaller and isolated pores. These changes are likely the result of ice expansion and soil grain displacement during the FTCs. While several authors have hypothesized that additional flow paths are created by FTCs (Mohanty et al., 2014; Muthanna et al., 2008), to date, direct supporting evidence remained limited. In addition, increased permeability due to increased pore connectivity under ice expansion, as shown for example in Al-Houri et al. (2009), Chamberlain and Gow (1979), Eigenbrod (1996) and Viklander (1998), has mainly been shown for natural, less sandier soils than typically used in bioretention systems.

The results obtained here in controlled laboratory experiments will have to be verified in the field under *in situ* conditions and as a function of the age of bioretention cells. In particular, the role of vegetation needs to be further determined. For example, zones of high vegetation density and thick plant roots may leave cavities after plant root decay, hence contributing to the soil porosity structure and providing preferential pathways for water infiltration (Le Coustumer et al., 2012; Valtanen et al., 2017).

4.2 Nutrient elimination: nitrate

In both the CC maintained at room temperature and the EC subjected to FTCs the injected NO_3^- and PO_4^{3-} were almost completely eliminated from the pore solutions draining out of the columns. High elimination efficiencies of NO_3^- have been observed for bioretention cells with an internal water storage zone in temperate climate conditions (Dietz and Clausen, 2006; Hunt et al., 2006; Kim et al., 2003; Li and Davis, 2014; Passeport et al., 2009). For example, with a similar initial NO_3^- concentration of 20 mg/L, Yang et al. (2013) report NO_3^- removal efficiencies of 91%, for a biphasic saturated – unsaturated bioretention system. However, the greater than 96% NO_3^- removal observed here for the EC is surprisingly high considering that NO_3^- removal tends to be very temperature sensitive, with usually higher activity in warmer compared to colder months (Khan et al., 2012b; Passeport et al., 2009). The long retention time tested, 4 days, was likely the main factor that enhanced nitrate removal despite the low temperatures.

Similar to Br^-, NO_3^- is not expected to significantly adsorb to the bioretention soil. Rather, the main processes responsible for the elimination of NO_3^- in bioretention cells are likely plant- and microbe-driven. Zones with high vegetation can lead to seasonally high NO_3^- removal rates due to root uptake (Lucas and Greenway, 2008; Valtanen et al., 2017). However, in the column experiments live plants were excluded, in order to better represent the no-growth winter conditions. Microbially-mediated processes are therefore the most plausible explanation for the consumption of NO_3^- in both columns. This is consistent with the microbial activity linked to the degradation of organic matter inferred from the chemical data-series for the drainage outflows, the porewater profiles, as well as the solid-phase chemistry.

A variety of microorganisms can produce or consume NO_3^-, while DON, a major component of the aqueous N in the present study, can significantly impact nitrogen cycling in bioretention cells (Li and Davis, 2014). Ammonification of organic nitrogen produces ammonium, which can further nitrify to NO_3^-. However, nitrification has a high theoretical oxygen demand of 4.57 g O_2/g NH_4-N, and an observed oxygen demand of about half the theoretical value in treatment wetland systems (Kadlec and Wallace, 2008). No data exist for the actual stoichiometry of ammonium nitrification to NO_3^- in bioretention systems, but the oxygen demand can be expected to be of the same order of magnitude as measured in wetlands, especially for bioretention cells with an internal storage zone as simulated here. Given that the two columns were fully saturated for 4 days before draining was initiated, it is unlikely that much oxygen was available to support nitrification. Thus, the discussion focuses primarily on possible NO_3^- consumption pathways.

Previous studies have shown that the water retention time is a key parameter to support microbial activity and enhance NO_3^- removal, in particular in colder months (Chen et al., 2013; Lucas and Greenway, 2008; Passeport et al., 2009). The results here show that dissimilatory Mn, Fe and SO_4^{2-} reduction coupled to organic matter degradation occurred while the columns were water-saturated, thus indicating the dominance of anaerobic microbial activity. Anaerobic microbial processes affecting N include dissimilatory NO_3^- reduction to ammonium (DNRA), anaerobic ammonium oxidation (Anammox), and denitrification. The low TDN concentrations in both columns, mainly consisting on DON, imply a net loss of aqueous N, likely as the gaseous species N_2 and N_2O. This in turn argues against a major role for DNRA, which would not cause a decrease in TDN.

Anammox can be a major sink of aqueous N in marine sediments and other environments (Francis et al., 2007). Anammox bacteria have also been detected in several water treatment systems such as wetlands (Erler et al., 2008; Humbert et al., 2012). However, contrary to denitrification, Anammox is not directly coupled to organic matter degradation. The observed decreases in DOC and TOC concentrations with time thus suggest that denitrification is likely the main process responsible for the removal of NO_3^- in the two columns. The high NO_3^--N concentrations injected, i.e., 5.65 mg NO_3^--N/L, the moderately high soil organic carbon content, up to 80 mg/g (i.e., 8%), and the anaerobic conditions during the water-saturated periods are all conducive to denitrification. Future work involving molecular biology and isotopic signatures would be particularly helpful to confirm the proposed dominant role of denitrification.

Rezanezhad et al. (2017) studied the effect of FTCs on NO_3^- consumption in peat soils. The authors showed that large macropores accelerate the delivery of NO_3^- to denitrifying organisms that preferentially reside in immobile regions such as smaller and isolated pores. They demonstrated that when the volume of immobile porewater increases, as found for the EC, denitrification rates increase due to enhanced diffusive exchange of NO_3^- between mobile and immobile pore domains. Thus, the FTC-induced changes in the pore structure (i.e., more connected large pores and more smaller pores) may represent an additional factor promoting denitrification in the EC. The interactions between soil structure and microbial activity in bioretention cells clearly deserves further attention.

4.3 Nutrient elimination: phosphate

Phosphorus elimination from stormwater runoff in bioretention cells mainly occurs via adsorption onto soil particle surfaces (Hunt et al., 2012; Li and Davis, 2016; Yan et al., 2016). This is also the case in this study and explains the increase in soil TP concentrations in the CC and EC relative to the initial column, indicating P accumulation in the soil matrix following the repeated injections of the solution. Phosphate is likely removed via adsorption onto the iron and aluminum oxides that were added to the bioretention soil, as well as the top mulch layer. While phosphorus can be retained by fixation to Fe(III) oxides under aerobic conditions, reducing conditions usually lead to phosphorus release because of the reductive dissolution of Fe(III) to Fe(II) (Boström et al., 1988; Parsons et al., 2017). Despite the strong reducing conditions imposed, TDP removal remained high for the entire duration of the experiment. This may indicate that a significant fraction of PO_4^{3-} adsorption took place on the aluminum oxides, which are not affected by changes in redox conditions. As observed in other studies, our results show that while PO_4^{3-} was adsorbed in the top layers of the soil column, it was subsequently able to migrate to lower depths, likely due to the downward movement of P-laden soil particles (Hsieh et al., 2007). Despite the very high TDP removal capacity, above 98% in both columns, higher TDP porewater concentrations and lower TP soil concentrations imply less TDP adsorption in the upper half of the EC than the CC. Possibly, this is due to the creation of larger pores in the top portion of the EC by the FTCs, as well as the higher frequency of isolated small pores, both of which reduce the contact surface area available for porewater TDP to reach adsorption sites.

The above finding has important design implications. While several engineered bioretention media and amendments have proven efficient to enhance phosphorus

adsorption (Hunt et al., 2006; Liu and Davis, 2014; Lucas and Greenway, 2011; Yan et al., 2016), the soil matrix composition alone should not be the sole factor to be taken into consideration when optimizing TDP removal in areas where FTCs occur. As the pore size distribution may change because of the freezing and thawing of the soil, it may be prudent to design bioretention cells that are sufficiently deep so that a significant portion of the soil remains unfrozen at all times. In this study, approximately 40 cm of the bioretention soil remained unfrozen during the FTCs, which was sufficient to retain the porewater TDP infiltrating to the lower portion of the EC. As the freezing depth is typically less than 20 cm in most temperate cold climate regions (Henry, 2007), it can be expected that most currently selected bioretention soil depths, typically around 50 to 100 cm, would be sufficient to maintain high phosphorus retention in sub-boreal regions.

5. Conclusions

This study evaluated the nutrient removal capacity of bioretention cells during FTCs under temperate cold climate conditions. The results showed that consecutive FTCs result in larger pores and a higher frequency of small and isolated pores that, together, help maintain the high infiltration rates required for the proper hydrological functioning of bioretention cells. The presence of an internal water storage zone below the freezing front and a high hydraulic retention time were found efficient to create a favorable environment for the removal of NO_3^- by denitrification. The results also suggest that bioretention cells should be sufficiently deep in order to capture all aqueous PO_4^{3-}. In addition, a soil media with additives that are stable under reducing conditions, e.g., aluminum oxides, should be used

to sustain long-term phosphorus retention. Future studies should evaluate the performance of bioretention cells under a wider range of input NO_3^- and PO_4^{3-} concentrations, hydraulic retention times, and variable FTC frequency and intensity. Finally, FTC effects on soil structure, hydrology, and nutrient removal observed in the column studies should be evaluated at pilot and full field scales as well as over longer time periods.

Acknowledgements

We thank Tilak Dutta and Yue Li from the Toronto Rehabilitation Institute for providing the snow. We are grateful to Dragana Simon and Jenny Hill from the Civil and Mineral Engineering department at the University of Toronto for providing help in the soil particle size analysis and K_{sat} measurements, and Marianne Vandergriendt, Sarah Legemaate, and Tatjana Milojevic from the Earth and Environmental Science department at the University of Waterloo for assisting during sample laboratory analysis. We are thankful to Jaime Douglas from J. Jenkins and Son Construction and Chris Denich from AquaforBeech for their support on the NSERC grants, and the Town of Ajax for access to the bioretention site.

Funding

This research was supported by the University of Toronto, Natural Science and Engineering Research Council (NSERC) Engage (#485238-15), Strategic (#479034-15), and Canada Research Chair (#950-230892) grants to E. Passeport, an NSERC Discovery grant (#RGPIN-2015-03801) to F. Rezanezhad, and the Canada Excellence Research Chair program to P. Van Cappellen.

The authors declare no competing interests.

Appendix A. Supplementary Material

The following is the supplementary material related to this article: xxx.

Appendix B. Videos

Two videos, one from the CC and one for the EC, representing a dynamic rotation of the 3D view of the X-ray tomography analyses of each sample, are available online: xxx.

References

Al-Houri ZM, Barber ME, Yonge DR, Ullman JL, Beutel MW. Impacts of frozen soils on the performance of infiltration treatment facilities. Cold Regions Science and Technology 2009; 59: 51-57.

Blecken GT, Zinger Y, Deletic A, Fletcher TD, Hedstrom A, Viklander M. Laboratory study on stormwater biofiltration: Nutrient and sediment removal in cold temperatures. Journal of Hydrology 2010; 394: 507-514.

Boström B, Andersen JM, Fleischer S, Jansson M. Exchange of phosphorus across the sediment-water interface. Hydrobiologia 1988; 170: 229-244.

Campbell JL, Mitchell MJ, Groffman PM, Christenson LM, Hardy JP. Winter in northeastern North America: a critical period for ecological processes. Frontiers in Ecology and the Environment 2005; 3: 314-322.

Chamberlain EJ, Gow AJ. Effect of freezing and thawing on the permeability and structure of soils. Engineering Geology 1979; 13: 73-92.

Chen XL, Peltier E, Sturm BSM, Young CB. Nitrogen removal and nitrifying and denitrifying bacteria quantification in a stormwater bioretention system. Water Research 2013; 47: 1691-1700.

Christensen AF, He H, Dyck MF, Lenore Turner E, Chanasyk DS, Naeth MA, et al. In situ measurement of snowmelt infiltration under various topsoil cap thicknesses on a reclaimed site. Canadian Journal of Soil Science 2013; 93: 497-510.

Christensen S, Christensen BT. Organic matter available for denitrification in different soil fractions: effect of freeze thaw/cycles and straw disposal. Journal of Soil Science 1991; 42: 637-647.

Conant B. Delineating and quantifying ground water discharge zones using streambed temperatures. Ground Water 2004; 42: 243-257.

Couture RM, Wallschlager D, Rose J, Van Cappellen P. Arsenic binding to organic and inorganic sulfur species during microbial sulfate reduction: a sediment flow-through reactor experiment. Environmental Chemistry 2013; 10: 285-294.

Denich C, Bradford A, Drake J. Bioretention: assessing effects of winter salt and aggregate application on plant health, media clogging and effluent quality. Water Quality Research Journal of Canada 2013; 48: 387-399.

Dhalla S, Zimmer C. Low Impact Development Stormwater Management Planning and Design Guide. Toronto and Toronto Region Conservation Authority, available from https://cvc.ca/wp-content/uploads/2014/04/LID-SWM-Guide-v1.0_2010_1_no-appendices.pdf, last accessed 2018/01/29 2010: 111-136.

Dietz ME, Clausen JC. Saturation to improve pollutant retention in a rain garden. Environmental Science & Technology 2006; 40: 1335-1340.

Eigenbrod KD. Effects of cyclic freezing and thawing on volume changes and permeabilities of soft fine grained soils. Canadian Geotechnical Journal 1996; 33: 529-537.

Erler DV, Eyre BD, Davison L. The contribution of Anammox and denitrification to sediment N2 production in a surface flow constructed wetland. Environmental Science & Technology 2008; 42: 9144-9150.

Fach S, Engelhard C, Wittke N, Rauch W. Performance of infiltration swales with regard to operation in winter times in an Alpine region. Water Science and Technology 2011; 63: 2658-2665.

Fenchel T, King GM, Blackburn TH. Chapter 6: Biogeochemical cycling in soils. Bacterial biogeochemistry: the ecophysiology of mineral cycling, Third Edition. Elsevier, London, UK, 2012, pp. 89-120.

Francis CA, Beman JM, Kuypers MMM. New processes and players in the nitrogen cycle: the microbial ecology of anaerobic and archaeal ammonia oxidation. ISME Journal 2007; 1: 19-27.

Gunther F. Water wells and ground water supplies in Ontario, Ontario Ministry of the Environment Report ISBN 0-7743-5072-5, 1980, pp. 105 pages.

Géhéniau N, Fuamba M, Mahaut V, Gendron MR, Dugué M. Monitoring of a rain garden in cold climate: case study of a parking lot near Montréal. Journal of Irrigation and Drainage Engineering 2015; 141: 04014073.

Hayashi M. The cold vadose zone: Hydrological and ecological significance of frozen-soil processes. Vadose Zone Journal 2013; 12.

He H, Dyck MF, Si BC, Zhang T, Lv J, Wang J. Soil freezing–thawing characteristics and snowmelt infiltration in Cryalfs of Alberta, Canada. Geoderma Regional 2015; 5: 198-208.

Henry HAL. Soil freeze-thaw cycle experiments: Trends, methodological weaknesses and suggested improvements. Soil Biology & Biochemistry 2007; 39: 977-986.

Hsieh CH, Davis AP, Needelman BA. Bioretention column studies of phosphorus removal from urban stormwater runoff. Water Environment Research 2007; 79: 177-184.

Humbert S, Zopfi J, Tarnawski SE. Abundance of anammox bacteria in different wetland soils. Environmental Microbiology Reports 2012; 4: 484-490.

Hunt WF, Davis AP, Traver RG. Meeting hydrologic and water quality goals through targeted bioretention design. Journal of Environmental Engineering 2012; 138: 698-707.

Hunt WF, Jarrett AR, Smith JT, Sharkey LJ. Evaluating bioretention hydrology and nutrient removal at three field sites in North Carolina. Journal of Irrigation and Drainage Engineering 2006; 132: 600-608.

Kadlec RH, Wallace SD. Treatment Wetlands, Second Edition, pp. 267-348. Boca Raton, FL: CRC Press, Taylor and Francis Group, 2008.

Kakuturu SP, Clark SE. Clogging mechanism of stormwater filter media by NaCl as a deicing salt. Environmental Engineering Science 2015; 32: 141-152.

Khan UT, Valeo C, Chu A, van Duin B. Bioretention cell efficacy in cold climates: Part 1—hydrologic performance. Canadian Journal of Civil Engineering 2012a; 39: 1210-1221.

Khan UT, Valeo C, Chu A, van Duin B. Bioretention cell efficacy in cold climates: Part 2—water quality performance. Canadian Journal of Civil Engineering 2012b; 39: 1222-1233.

Kim HH, Seagren EA, Davis AP. Engineered bioretention for removal of nitrate from stormwater runoff. Water Environment Research 2003; 75: 355-367.

Kratky H, Li Z, Chen YJ, Wang CJ, Li XF, Yu T. A critical literature review of bioretention research for stormwater management in cold climate and future

research recommendations. Frontiers of Environmental Science & Engineering 2017; 11.
Le Coustumer S, Fletcher TD, Deletic A, Barraud S, Poelsma P. The influence of design parameters on clogging of stormwater biofilters: A large-scale column study. Water Research 2012; 46: 6743-6752.
Lee JH, Bang KW. Characterization of urban stormwater runoff. Water Research 2000; 34: 1773-1780.
Li H, Davis AP. Urban particle capture in bioretention media. I: Laboratory and field studies. Journal of Environmental Engineering 2008; 134: 409-418.
Li JK, Davis AP. A unified look at phosphorus treatment using bioretention. Water Research 2016; 90: 141-155.
Li LQ, Davis AP. Urban stormwater runoff nitrogen composition and fate in bioretention systems. Environmental Science & Technology 2014; 48: 3403-3410.
Liu JY, Davis AP. Phosphorus speciation and treatment using enhanced phosphorus removal bioretention. Environmental Science & Technology 2014; 48: 607-614.
Lucas WC, Greenway M. Nutrient retention in vegetated and nonvegetated bioretention mesocosms. Journal of Irrigation and Drainage Engineering 2008; 134: 613-623.
Lucas WC, Greenway M. Phosphorus retention by bioretention mesocosms using media formulated for phosphorus sorption: Response to accelerated loads. Journal of Irrigation and Drainage Engineering 2011; 137: 144-153.
Ma W, Zhang LH, Yang CS. Discussion of the applicability of the generalized Clausius-Clapeyron equation and the frozen fringe process. Earth-Science Reviews 2015; 142: 47-59.
Matzner E, Borken W. Do freeze-thaw events enhance C and N losses from soils of different ecosystems? A review. European Journal of Soil Science 2008; 59: 274-284.
Moghadas S, Gustafsson AM, Viklander P, Marsalek J, Viklander M. Laboratory study of infiltration into two frozen engineered (sandy) soils recommended for bioretention. Hydrological Processes 2016; 30: 1251-1264.
Mohanty SK, Saiers JE, Ryan JN. Colloid-facilitated mobilization of metals by freeze-thaw cycles. Environmental Science & Technology 2014; 48: 977-984.
Muthanna TM, Viklander M, Gjesdahl N, Thorolfsson ST. Heavy metal removal in cold climate bioretention. Water Air and Soil Pollution 2007; 183: 391-402.
Muthanna TM, Viklander M, Thorolfsson ST. Seasonal climatic effects on the hydrology of a rain garden. Hydrological Processes 2008; 22: 1640-1649.
O'Neill SW, Davis AP. Water treatment residual as a bioretention amendment for phosphorus. II: Long-term column studies. Journal of Environmental Engineering 2012; 138: 328-336.
OECD. Organisation for Economic Co-operation and Development (OECD). Test guideline 312: Leaching in soil columns. OECD Publishing, 2004, pp. 15.
Parsons CT, Rezanezhad F, O'Connell DW, Van Cappellen P. Sediment phosphorus speciation and mobility under dynamic redox conditions. Biogeosciences 2017; 14: 3585-3602.

Passeport E, Hunt WF, Line DE, Smith RA, Brown RA. Field study of the ability of two grassed bioretention cells to reduce storm-water runoff pollution. Journal of Irrigation and Drainage Engineering 2009; 135: 505-510.

Rezanezhad F, Kleimeier C, Milojevic T, Liu H, Weber TKD, Van Cappellen P, et al. The role of pore structure on nitrate reduction in peat soil: A physical characterization of pore distribution and solute transport. Wetlands 2017: 1-10.

Rickard D, Luther GW. Chemistry of iron sulfides. Chemical Reviews 2007; 107: 514-562.

Roseen RM, Ballestero TP, Houle JJ, Avellaneda P, Briggs J, Fowler G, et al. Seasonal performance variations for storm-water management systems in cold climate conditions. Journal of Environmental Engineering 2009; 135: 128-137.

Roy-Poirier A, Champagne P, Filion Y. Review of bioretention system research and design: Past, present, and future. Journal of Environmental Engineering 2010; 136: 878-889.

Stevenson FJ. The sulfur cycle. Cycles of soil : carbon, nitrogen, phosphorus, sulfur, micronutrients. Wiley, New York, USA, 1986, pp. 330 - 368.

Valtanen M, Sillanpaa N, Setala H. A large-scale lysimeter study of stormwater biofiltration under cold climatic conditions. Ecological Engineering 2017; 100: 89-98.

Viklander P. Permeability and volume changes in till due to cyclic freeze/thaw. Canadian Geotechnical Journal 1998; 35: 471-477.

Yan Q, Davis AP, James BR. Enhanced organic phosphorus sorption from urban stormwater using modified bioretention media: Batch studies. Journal of Environmental Engineering 2016; 142.

Yang HB, Dick WA, McCoy EL, Phelan PL, Grewal PS. Field evaluation of a new biphasic rain garden for stormwater flow management and pollutant removal. Ecological Engineering 2013; 54: 22-31.

Zhai C, Wu SL, Liu SM, Qin L, Xu JZ. Experimental study on coal pore structure deterioration under freeze-thaw cycles. Environmental Earth Sciences 2017; 76.

Zhang W, Brown GO, Storm DE, Zhang H. Fly-ash-amended sand as filter media in bioretention cells to improve phosphorus removal. Water Environment Research 2008; 80: 507-516.

Table 1: Pore characteristics in the soil samples from the experimental and control columns.

	Control Column	**Experimental Column**
Soil dimension (voxels)	902×902×490	880×880×450
Bulk volume (mm^3)	906.5	792.4
Number of pores	888,797	952,047
Porosity (%)	39.8	32.5
Specific surface (mm^2/mm^3 bulk)	12.4	7.4
Average pore hydraulic radius (mm)	0.032	0.044
Average spatial pore density (counts/mm^2 bulk/slice)	12.9	15.8
Average pore area (μm^2)	1.41×10^4	1.76×10^4
Minimum pore area (μm^2)[(a)]	1.73×10^2	1.73×10^2
Median pore area (μm^2)	1.38×10^3	1.04×10^3
Maximum pore area (μm^2)	2.65×10^6	3.88×10^6

[(a)] Note that the minimum pore size, 1.73×10^2 μm^2 was determined by the image resolution, which was the same for both samples.

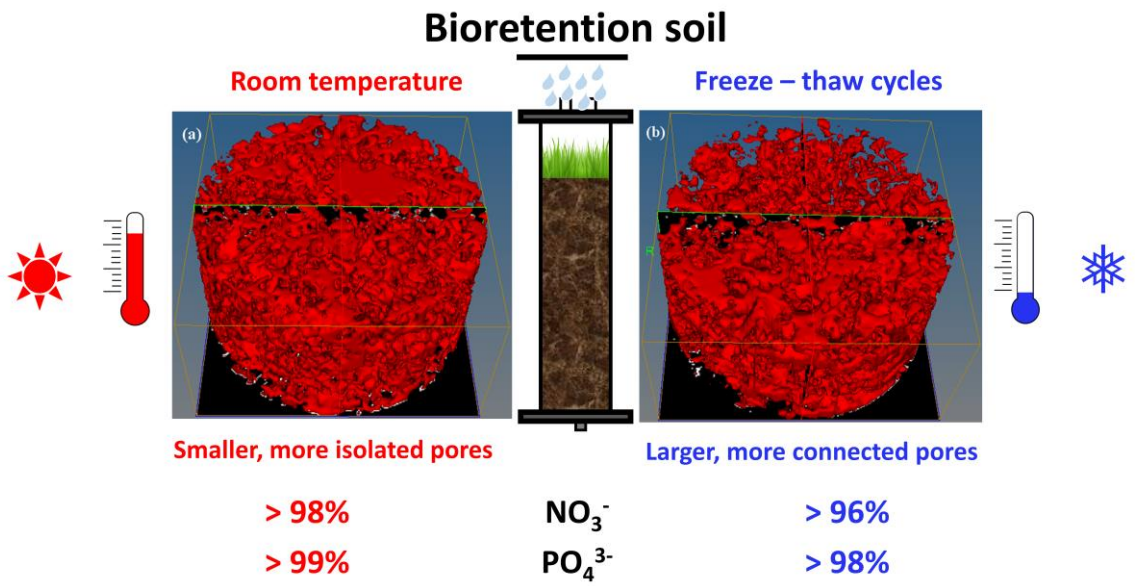

Graphical abstract

Highlights

- Effects of freeze-thaw cycles (FTCs) on bioretention performance were assessed
- Column experiments were conducted with soil from an active bioretention cell
- FTCs resulted in larger pores and more small pores maintaining high infiltration
- Very high nitrate and phosphate removal was observed in the soil columns
- With proper design, bioretention cells are efficient under cold winter conditions

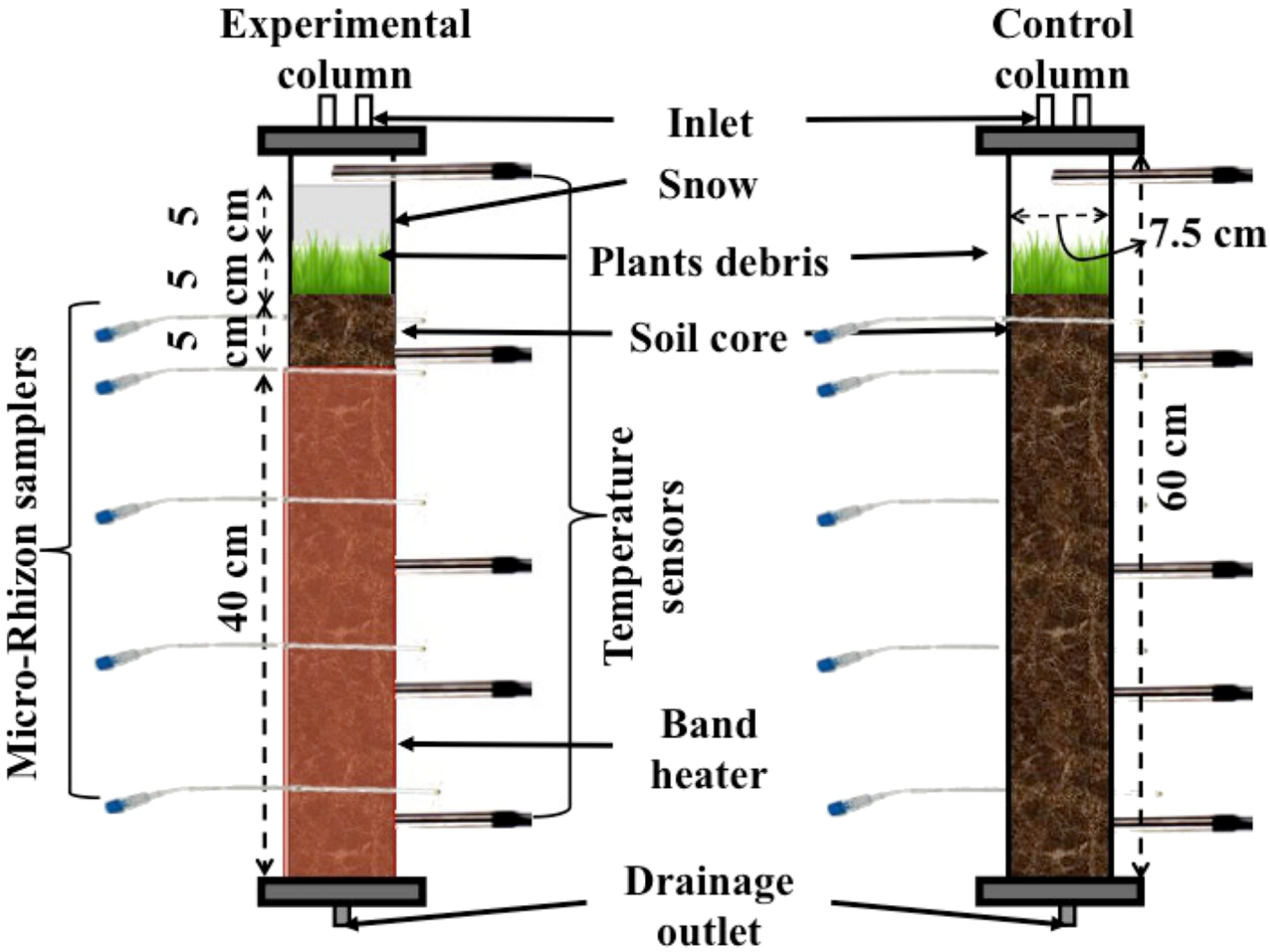
Experimental column
Control column
Inlet
Snow
Plants debris
Soil core
Band heater
Drainage outlet
Micro-Rhizon samplers
Temperature sensors
5 cm
5 cm
5 cm
40 cm
7.5 cm
60 cm

Figure 1

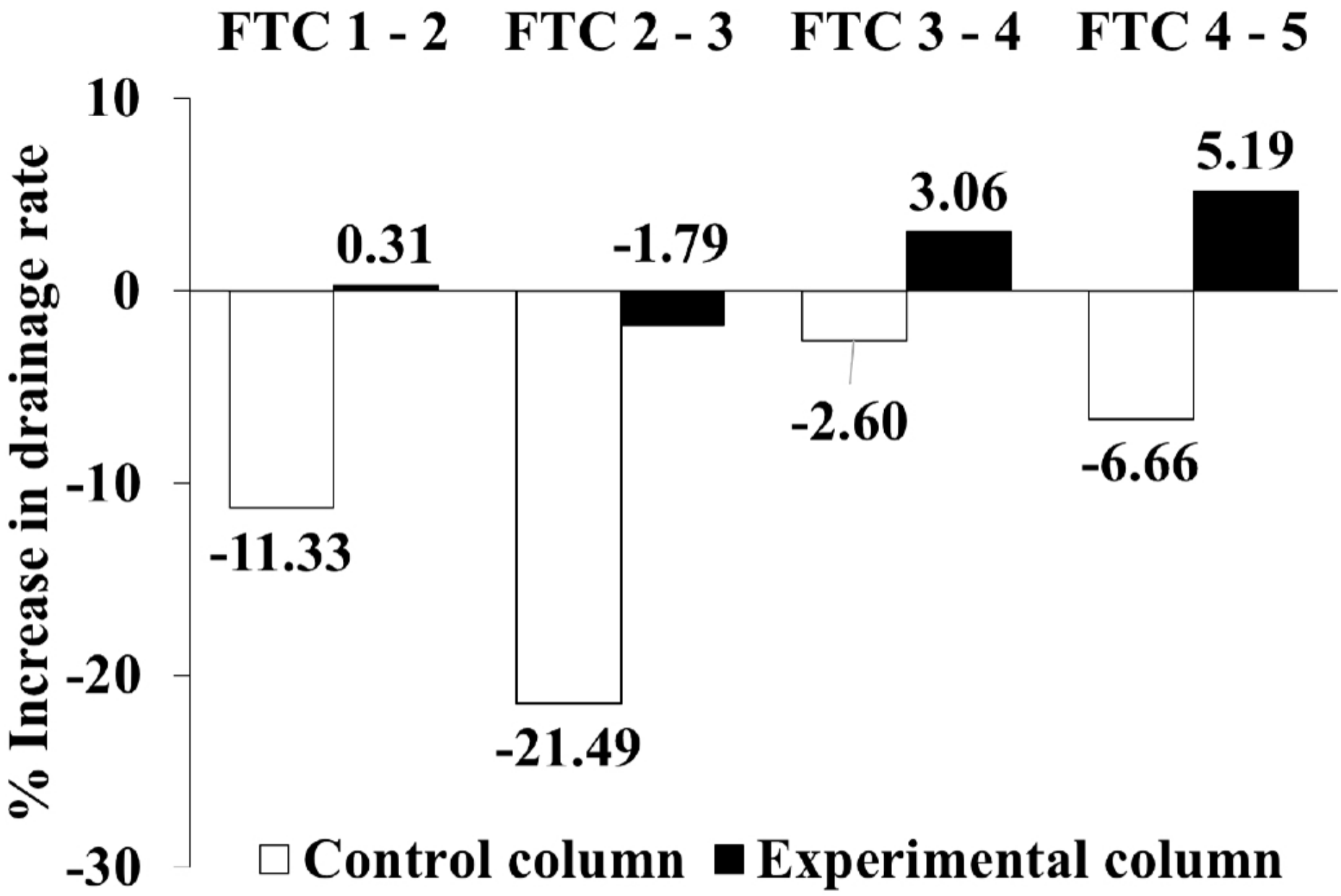
FTC 1 - 2
FTC 2 - 3
FTC 3 - 4
FTC 4 - 5
10
0
-10
-20
-30
% Increase in drainage rate
0.31
-1.79
3.06
5.19
-11.33
-21.49
-2.60
-6.66
Control column
Experimental column

Figure 2

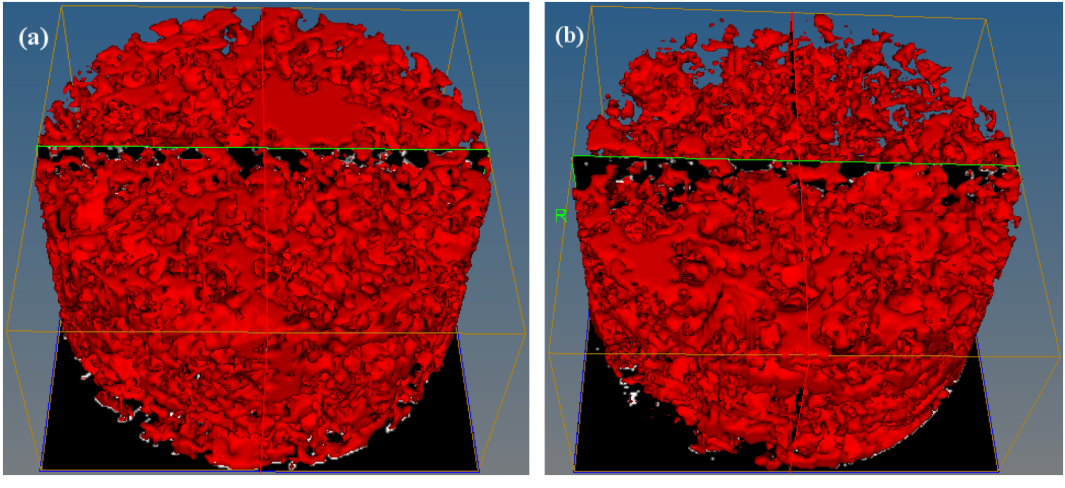

Figure 3

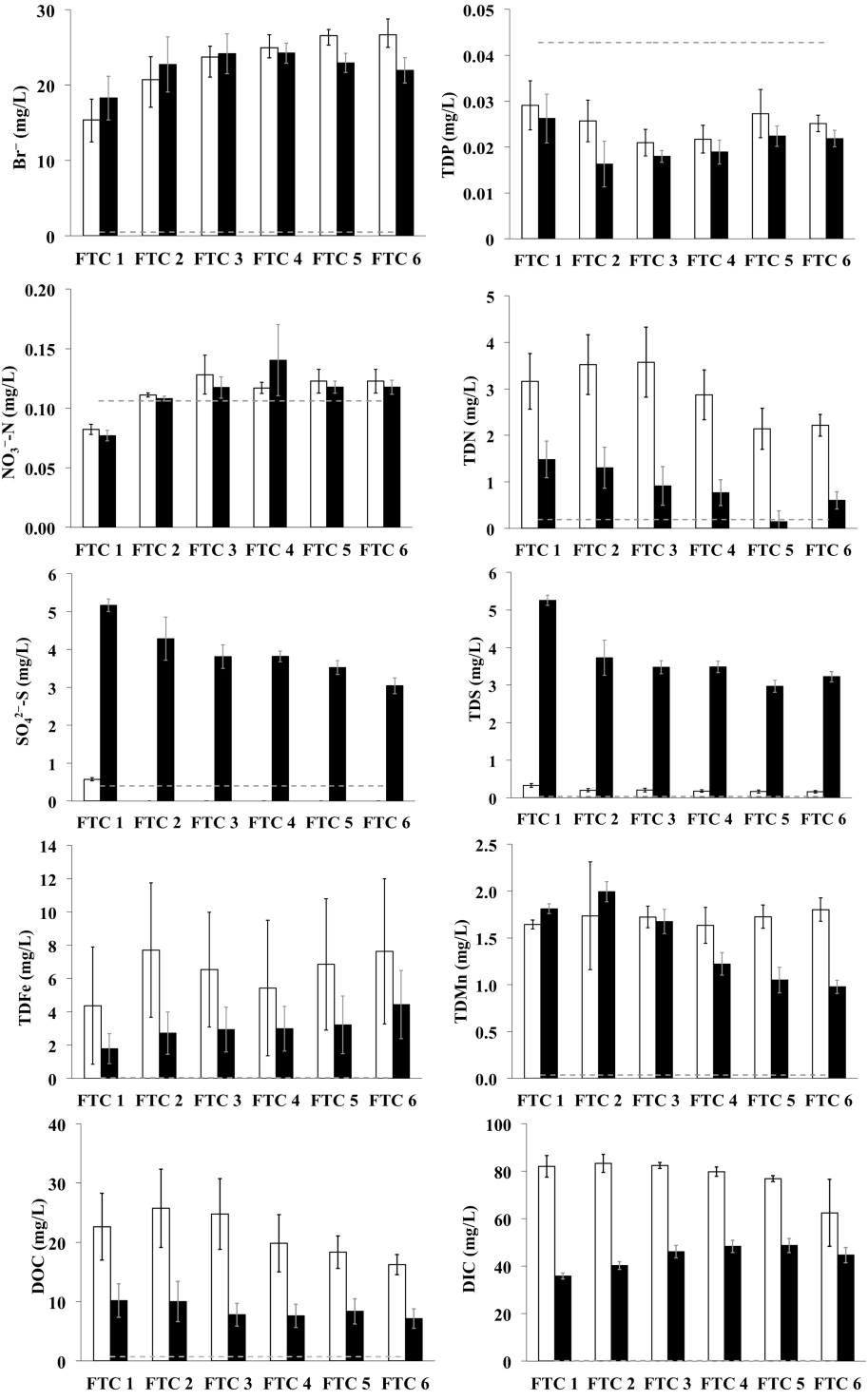
Br⁻ (mg/L)
TDP (mg/L)
NO3-N (mg/L)
TDN (mg/L)
SO4 2--S (mg/L)
TDS (mg/L)
TDFe (mg/L)
TDMn (mg/L)
DOC (mg/L)
DIC (mg/L)
FTC 1 FTC 2 FTC 3 FTC 4 FTC 5 FTC 6

Figure 4

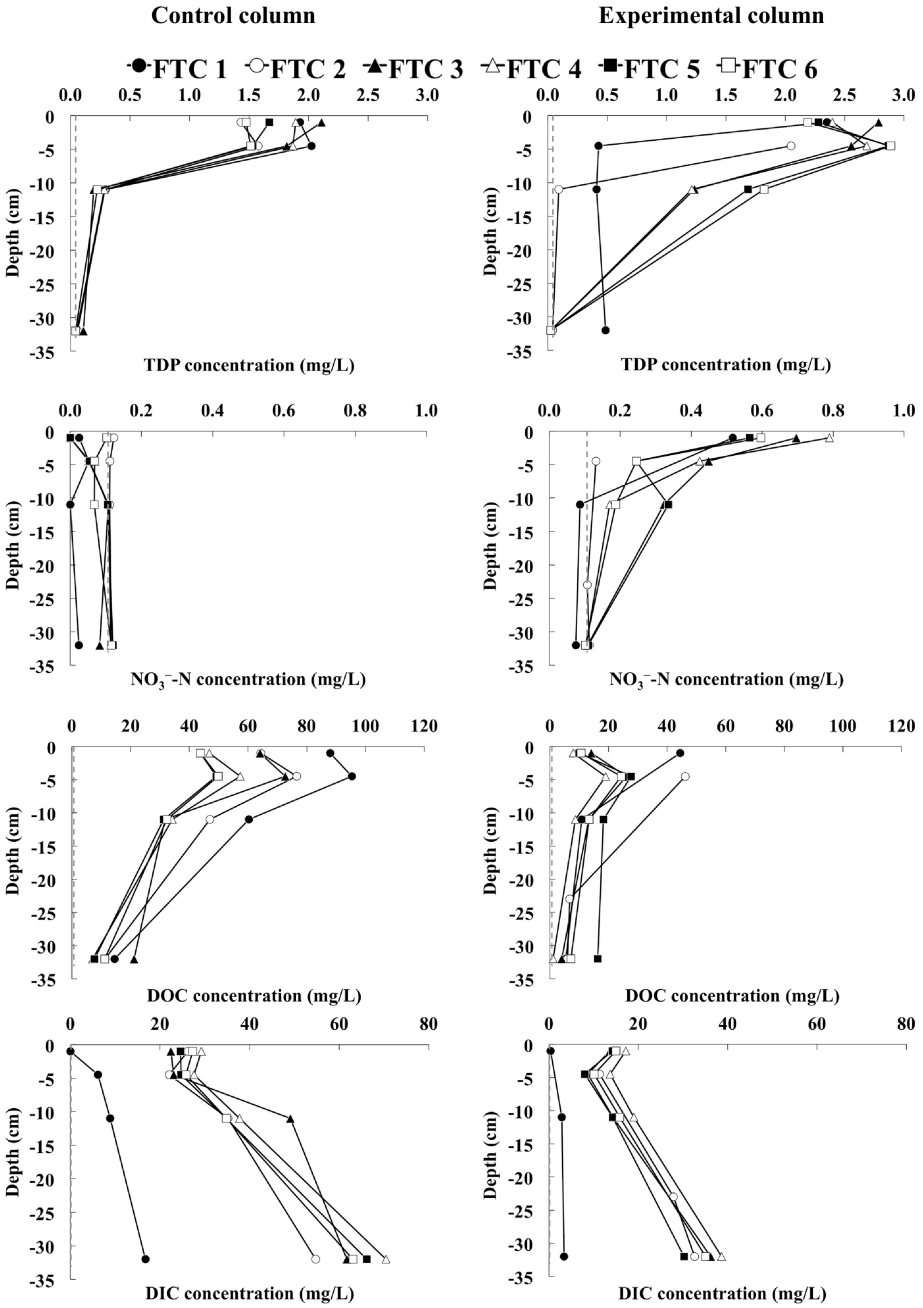
Control column
Experimental column
FTC 1
FTC 2
FTC 3
FTC 4
FTC 5
FTC 6
Depth (cm)
TDP concentration (mg/L)
NO3−-N concentration (mg/L)
DOC concentration (mg/L)
DIC concentration (mg/L)

Figure 5

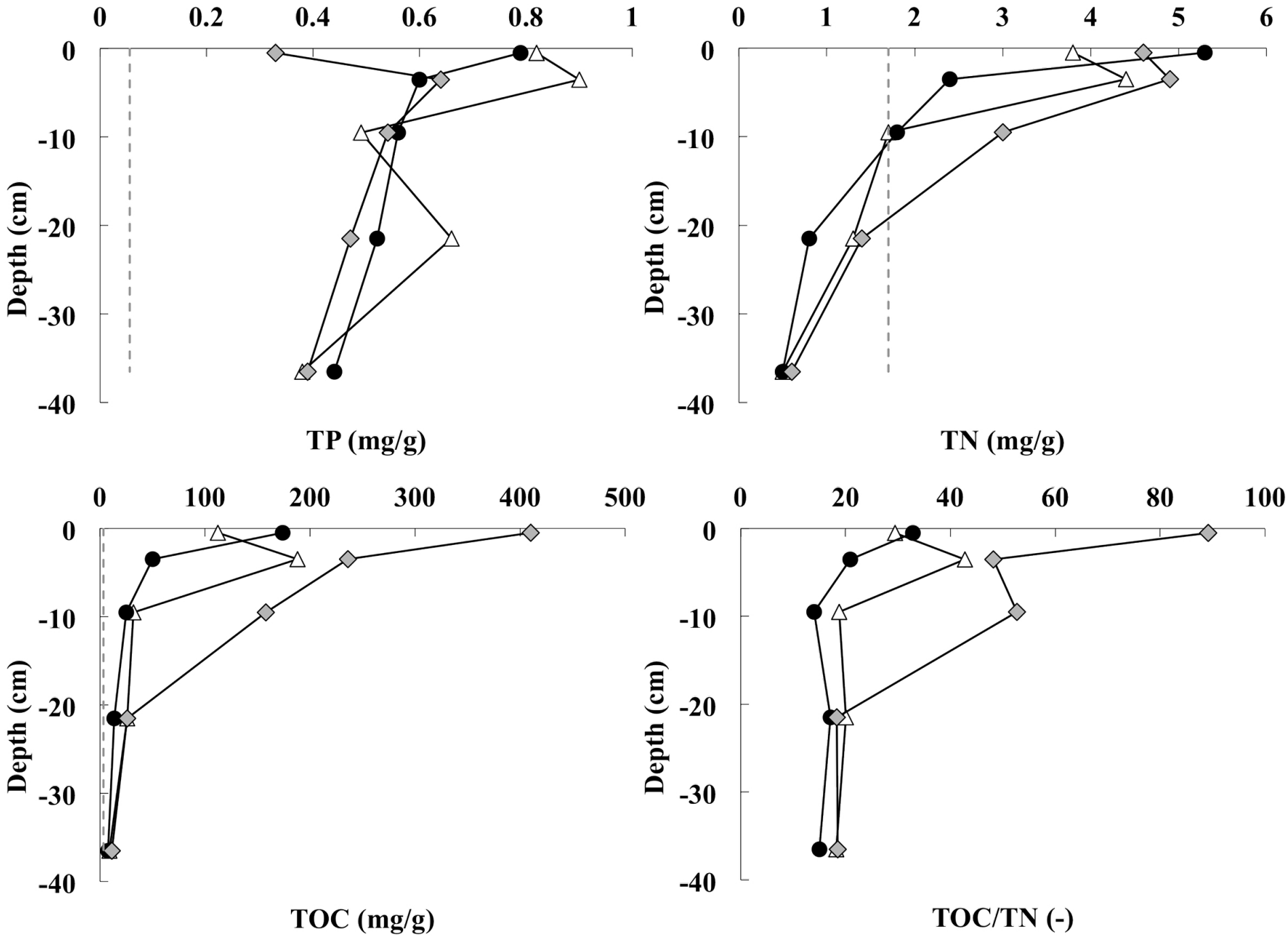
0
0.2
0.4
0.6
0.8
1
0
-10
-20
-30
-40
Depth (cm)
TP (mg/g)
0
1
2
3
4
5
6
TN (mg/g)
0
100
200
300
400
500
TOC (mg/g)
0
20
40
60
80
100
TOC/TN (-)

Figure 6